Model-based Control of a fast Rover over natural Terrain

D. Lhomme-Desages*, Ch. Grand*, J-C. Guinot*
*Laboratoire de Robotique de Paris
Route du Panorama, 92260 Fontenay-aux-Roses
email: lhomme@robot.jussieu.fr, grand@robot.jussieu.fr, guinot@robot.jussieu.fr

Abstract— **A model-based control for fast autonomous four-wheel mobile robots on soft soils is developed. This control strategy takes into account slip and skid effects to extend the mobility over planar granular soils. Each wheel is independently actuated by an electric motor. The overall objective is to follow a path roughly at relatively high speed. Some results obtained in dynamic simulation are presented.**

Keywords— **rover, slip control, skid-steering, wheel-soil interaction**

I. Introduction

Many popular controllers for wheeled mobile robots assume that wheels roll without slipping [1]. This leads to a nonholonomic constraint added to the kinematic or dynamic model. This assumption is quite legitimate for usual applications such as autonomous cars over hard terrains or slow indoor exploration. However, it is no longer adequate for many applications where wheel slip cannot be neglected [2], especially for traveling over natural soils at high speed [3]. Therefore, a new control scheme is required.

In this paper, a model-based control method for fast autonomous mobile robots on soft soils is developed. On such a type of terrain (sand for instance), slip and skid phenomena may be significant. The control strategy takes into account these effects to extend the mobility of the vehicles over planar natural soils.

A non-linear model-based control of wheel slippage is studied, using a semi-empirical wheel-soil interaction model. A higher-level control is applied to a four wheel skid-steering vehicle which can travel at relatively high speed (several meters per second). Each wheel is independently actuated by an electric motor.

The control frame is developed for a four-wheel mobile robot. The overall objective is to follow a path at relatively high speed. This controller implies a low-level control method that aims to regulate the slip rate of one wheel, since the traction force generated by the rotation of the wheel at the contact patch depends on the wheel slip. We indicate the limits and the sensors required to apply this strategy.

Finally, some results obtained in dynamic simulation are presented. We compare different kinematic structures (pure skid-steering and directional wheels). A comparison is also carried out with a classical kinematic control.

II. Wheel-soil contact model

Several modeling frameworks can be used to calculate the efforts involved in the wheel-soil interaction process. We use an extended version of the terramechanic model introduced by Bekker ([4],[5]). We assume a rigid wheel over a soft soil (Figure 1).

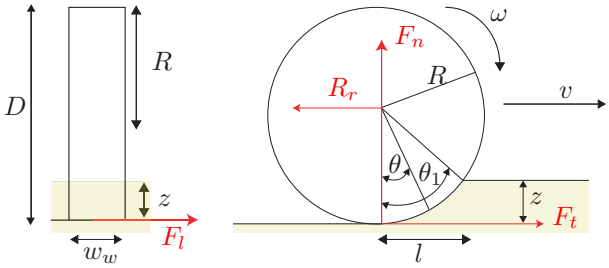

Fig. 1. Model of a rigid wheel

v is the velocity of the center of the wheel. ω is the angular velocity of the wheel. In this model, the efforts depend on the slip rate s, which is defined as:

$$s = \begin{cases} 1 - \frac{v}{\omega . R} & if \quad R\omega \geq v \\ 1 - \frac{\omega . R}{v} & if \quad R\omega < v \end{cases} \tag{1}$$

for $v > 0$ and $\omega > 0$. This definition can be extended to every $(v, \omega) \in \Re^2$, as it is shown on Figure 2.

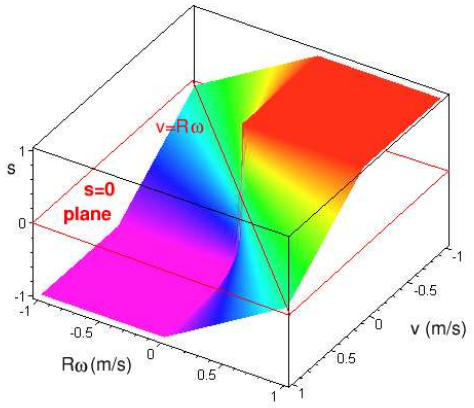

Fig. 2. slip rate as a function of v and $R\omega$

v is the linear velocity of the center of the wheel. ω is the angular velocity of the wheel.

According to Bekker theory [4], the normal force depends on the sinkage z through:

$$F_n = \frac{1}{3}\left[w_w \left(\frac{k_c}{b} + k_\phi\right)(3-n)\sqrt{D} z^{\frac{2n+1}{2}}\right] \tag{2}$$

where k_c, k_ϕ and n are soil parameters. w_w is the width of the wheel. $b = \min(w_w, l)$, l being the length of the contact patch.

The tractive force is related to the slip rate:

$$F_t(s) = F_{tmax}\left[1 - \frac{K}{s.l}\left(1 - e^{-s.l/K}\right)\right] \tag{3}$$

where:

$$F_{tmax} = l w_w c + F_n \tan\phi \tag{4}$$

c, ϕ and K are soil parameters. The shape of F_t is plotted on Fig. 3 with parameters of Tab. I.

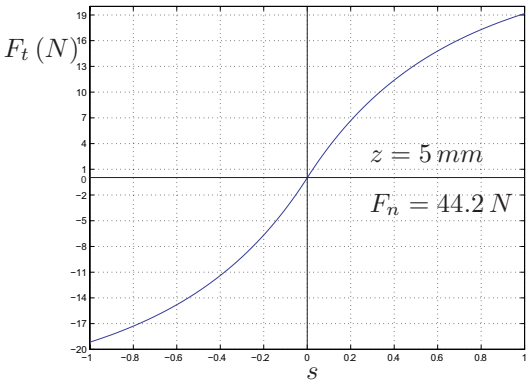

Fig. 3. Traction force vs slip rate

Additionally, the rolling resistance is assumed to be mainly caused by soil compaction:

$$R_r = w_w \frac{z^{n+1}}{n+1}\left(\frac{k_c}{b} + k_\phi\right) \tag{5}$$

Hence the net longitudinal force DP (drawbar pull) is given by:

$$DP(s) = F_t(s) - R_r \tag{6}$$

Lateral forces can be implemented, including bulldozing resistance, as described in [6]. In this study, we use a simple linearized Coulomb model for lateral forces. This contact model is being validated by experimental measurements on a testbed under development.

III. Modeling of a rover

The kinematic and geometric parameters of the vehicle is shown on figure 4.

A. Tractive force distribution

We note $\mathbf{F}$ the global vector of forces and torque applied to the center of mass of the platform, in the local frame attached to the chassis. this vector has two components since the lateral component F_Y is uncontrollable, thus ignored.

$$\mathbf{F} = \begin{bmatrix} F_X \\ M_\psi \end{bmatrix} \tag{7}$$

F_X is the longitudinal component of the force in the local frame. M_ψ is the global torque along the vertical

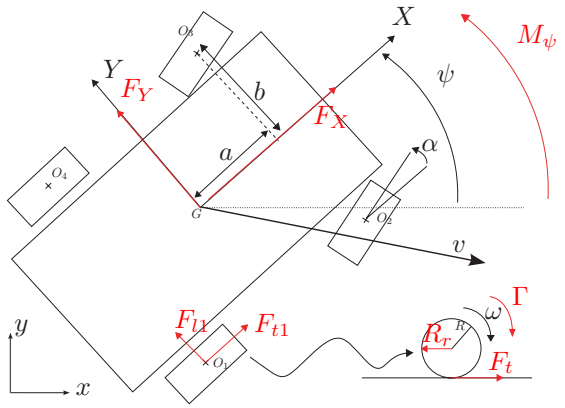

Fig. 4. Model of a four-wheel rover

axis. Each wheel is submitted to tangential lateral and longitudinal contact forces, gathered in corresponding vectors:

$$\mathbf{F_t} = [DP_1, DP_2, DP_3, DP_4]^T \tag{8}$$

$$\mathbf{F_l} = [F_{l1}, F_{l2}, F_{l3}, F_{l4}]^T \tag{9}$$

The position of the robot is the position of the center of mass of the chassis in the operational space:

$$\mathbf{X} = [x, y, \psi]^T$$

and θ is the vector of angular positions of the wheels.

For each wheel, we can separate the lateral and longitudinal forces, which are related to the global force by a linear equation:

$$\mathbf{F} = \tag{10}$$

To simplify, consider that only the two front wheels are directional and set by one angle α. The absence of the Ackerman kinematic model is also a simplification.

$$\mathbf{A_t} = \begin{bmatrix} 1 & \cos\alpha & \cos\alpha & 1 \\ b & b\cos\alpha + a\sin\alpha & -b\cos\alpha + a\sin\alpha & -b \end{bmatrix} \tag{11}$$

and:

$$\mathbf{A_l} = \begin{bmatrix} 0 & \sin\alpha & \sin\alpha & 0 \\ -a & a\cos\alpha - b\sin\alpha & a\cos\alpha + b\sin\alpha & -a \end{bmatrix} \tag{12}$$

Therefore, assuming translation and angular velocities are known, we can deduce the longitudinal forces to apply. Angular velocities can be easily measured via optical coders. Ground velocity can be estimated by a Doppler sensor for instance [7].

We can inverse the linear system (10) by minimizing the 2-norm of vector $\mathbf{Ft}$ (thus minimizing tractive efforts). Using the pseudo-inverse of $\mathbf{A_t}$, the optimal tractive efforts are computed from equation 13, where hats denote estimated values, and stars denote desired values:

$$\mathbf{F_t}^* = \widehat{\mathbf{A_t}}^+ \left(\mathbf{F}^* - \widehat{\mathbf{A_l}}\widehat{\mathbf{F_l}}\right) \tag{13}$$

The lateral efforts $\widehat{\mathbf{F_l}}$ are estimated with the contact model and a measure of the kinematic state of the vehicle. The pseudo-inverse of this matrix $\mathbf{A_t}$ is computable in a analytical way:

$$\widehat{\mathbf{A_t}}^{+} = \frac{1}{2(b^2\cos^4\alpha + 2b^2\cos^2\alpha + b^2 + a^2\sin^2\alpha)} \cdot \begin{bmatrix} b^2\cos^2\alpha - a\cos\alpha b\sin\alpha + b^2 + a^2\sin^2\alpha & -\cos\alpha a\sin\alpha + b + \cos^2\alpha b \\ -\left(\cos\alpha a\sin\alpha - b - \cos^2\alpha b\right) b\cos\alpha & b\cos^3\alpha + b\cos\alpha + a\sin\alpha \\ \left(\cos^2\alpha b + \cos\alpha a\sin\alpha + b\right) b\cos\alpha & -b\cos^3\alpha - b\cos\alpha + a\sin\alpha \\ b^2\cos^2\alpha + a\cos\alpha b\sin\alpha + b^2 + a^2\sin^2\alpha & -\cos^2\alpha b - \cos\alpha a\sin\alpha - b \end{bmatrix} \quad (14)$$

However, these tractive efforts can be unreachable if we consider the contact model. If the desired tractive force is non admissible by the soil ($F_t > F_{tmax}$), then the robot will be unable to follow the path precisely and will skid. A higher control loop is required to maintain the vehicle on a satisfying path.

B. Control architecture

Figure 5 presents the overall control system. The desired slip rate s^* is provided by the inversion of the estimated contact model from the desired traction force ${F_t}^*$. This force is computed from the global desired force by the dispatcher ${A_t}^+$, which requires an estimation of lateral forces. The role of the trajectory controller is to generate a proper desired global force.

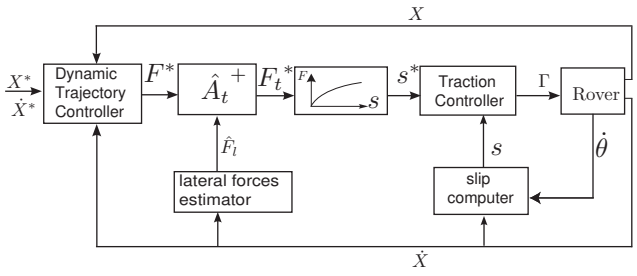

Fig. 5. Control block diagram

This architecture is composed of two stages, the traction control and the trajectory control, which are detailed in the next sections.

IV. Motion control

A. Traction controller

Several slip control methods exist in the literature, including nonlinear and gain-scheduled PID, sliding mode [8], fuzzy logic [9], or Lyapunov synthesis [10].

Simple slip control strategies have been used for several mobile robots in rough terrain ([11], [12]). Like these authors, we implement a simple PI-controller (Fig. 6). A derivative gain is inadequate since the slip rate is a discontinuous function. Each independent electric motor is controlled in torque (namely in current).

Numerical simulations have been led in a dynamical multibody modeling software [13] (Fig. 8). An extension has been developed to implement the teramechanic contact model. The curve 7 shows the result of the tracking of a step desired slip value of $0,8$ ($K_p = K_i = 100$).

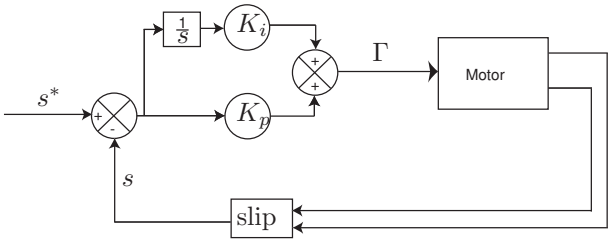

Fig. 6. Control block diagram with PI-controller

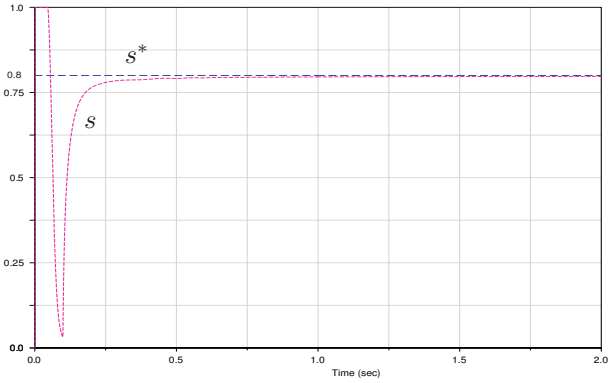

Fig. 7. Comparison between step desired and simulated slip rate with PI-control

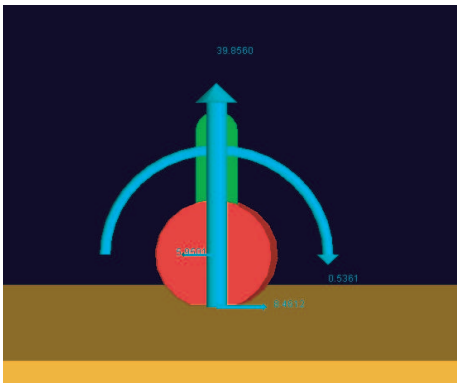

Fig. 8. Control of a one-wheel vehicle

B. Trajectory controller

The trajectory controller is a high-level module that drives the robot toward the desired path. It provides a desired global force depending on kinematic and geometric situation ($\mathbf{F}^* = f(\mathbf{X}, \dot{\mathbf{X}})$). A simple strategy may be defined as the following:

$${F_X}^* = k_{pX}\left(v^* - v\right) + k_{iX}\int\left(v^* - v\right) \quad (15)$$

where k_{iX} and k_{pX} are gains. This defines a PI-controller on operational velocity v.

Let d be the distance between the center of mass of the robot and the desired path.

The desired global torque is computed by:

$${M_\psi}^* = k_{p\psi}\left(\tilde{\psi} - \psi\right) + k_{i\psi}\int\left(\tilde{\psi} - \psi\right) + k_{d\psi}\left(\dot{\tilde{\psi}} - \dot{\psi}\right) \quad (16)$$

This is a PID-control of the heading angle ψ. The desired value $\tilde{\psi} = \psi^* - \gamma$ (effective desired heading) is the sum of the reference heading angle ψ^* and a correction depending on d and a gain k_f, computed by:

$$\gamma = atan(k_f d)$$

This allows the vehicle to go back to the desired path by adapting the desired heading.

V. Simulation results

To simulate the behavior of the robot, a simple desired trajectory has been chosen, which is a right bend after an acceleration phase at constant rate. The minimal radius of curvature is 54 cm. Kinematic, dynamical and contact parameters are given in the table I. Soil parameters correspond to a dry sandy soil [5]. Dynamic and geometrical parameters are taken from an existing robot.

TABLE I
Simulation parameters

m_r	$1\,kg$	wheel mass
m_c	$14\,kg$	chassis mass
J	$1.03.10^{-2}\,kg.m^2$	wheel inertia
R	$10\,cm$	wheel radius
w_w	$6\,cm$	wheel width
a	$35\,cm$	half wheelbase
b	$23\,cm$	half track width
n	0.705	soil exponent
k_c	$6940\,N.m^{-(n+1)}$	cohesive modulus
k_ϕ	$505800\,N.m^{-(n+2)}$	friction modulus
ϕ	31.5 deg	friction angle
c	$1150\,Pa$	cohesion
K	$1.15\,cm$	soil modulus
K_p	300	proportional gain
K_i	1000	integral gain

A passive revolute joint has been introduced between both sides of the platform to guarantee an isostatic contact.

A. Non-directional wheels

We consider in this section a pure skid-steering rover ($\alpha = 0$). The matrix 11 and 12 are now:

$$\mathbf{A_t} = \begin{bmatrix} 1 & 1 & 1 & 1 \\ b & b & -b & -b \end{bmatrix} \quad (17)$$

$$\mathbf{A_l} = \begin{bmatrix} 0 & 0 & 0 & 0 \\ -a & a & a & -a \end{bmatrix} \quad (18)$$

The heading of the robot can only be achieved by the difference between tractive forces of both sides of the chassis. We obtain the sequence of the figure 9.

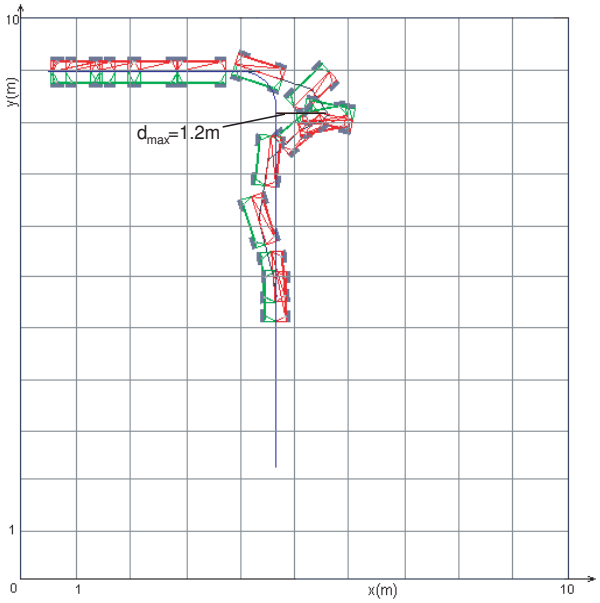

Fig. 9. Right bend (skid-steering)

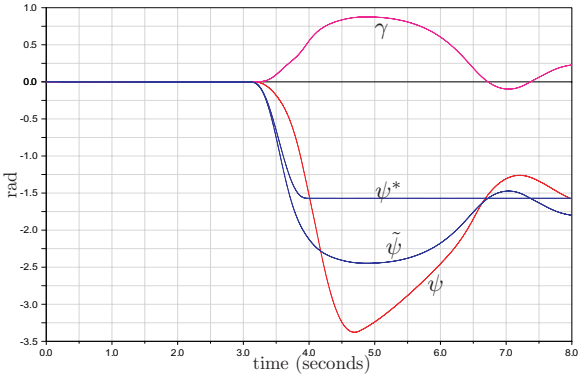

Fig. 10. Rover direction and desired heading (skid-steering)

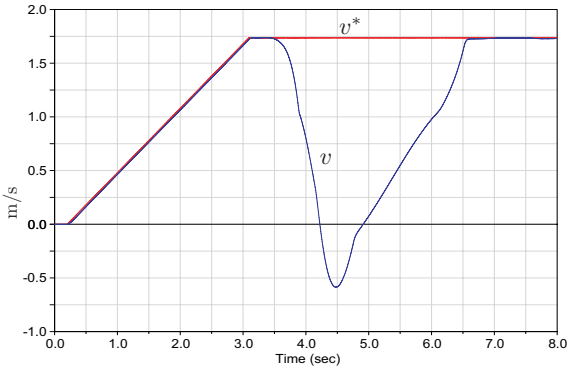

Fig. 11. Rover velocity (skid-steering)

B. Directional front wheels

A simple law is implemented for the steering:

$$\alpha = \psi^* - \psi \quad (19)$$

As shows the sequence of Fig. 12, the desired path is followed with a higher precision.

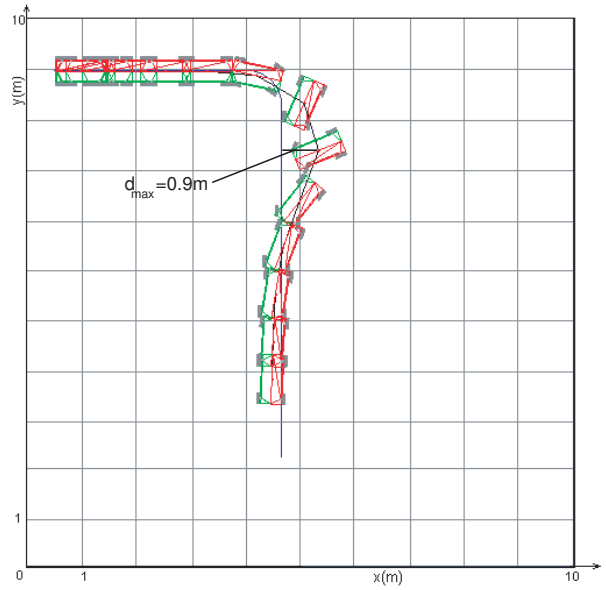

Fig. 12. Right bend (directional wheels)

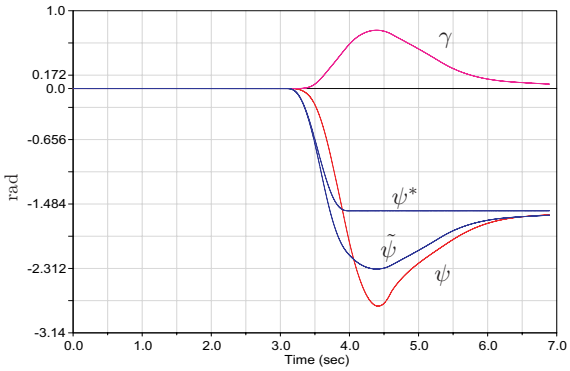

Fig. 13. Rover direction and desired heading (directional wheels)

C. Classical kinematic control

This control method consists in assuming the perfect rolling in the longitudinal direction ([1] for example). The platform longitudinal velocity and the rotation along the vertical axis are supposed to be determined by the angular velocities of the wheels.

Therefore:

$$\begin{aligned} {\omega_1}^* &= {\omega_2}^* = \left(v^* + b\dot{\tilde{\psi}}\right)/R \\ {\omega_3}^* &= {\omega_4}^* = \left(v^* - b\dot{\tilde{\psi}}\right)/R \end{aligned} \tag{20}$$

with:

$$v^* = v + K_k\,(p^* - p) \tag{21}$$

where p is the curvilinear abscis. K_k is a gain.

Wheels angular velocities are controlled by a PI-controller. Fig. 16 shows measured angular velocities.

The impact of slippage is clearly highlighted on the sequence 15. In this particular case, the robot slips laterally and fails to accomplish its path, although the tracking of the wheel velocities is fine. The system is unstable.

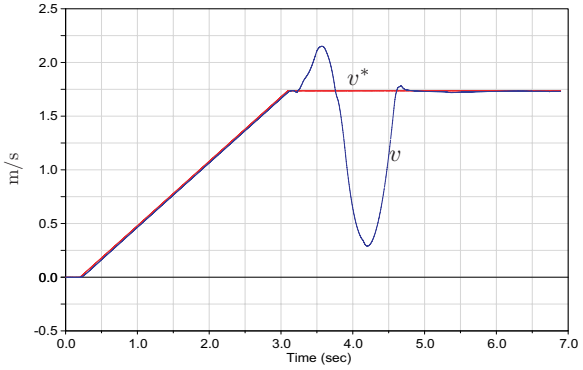

Fig. 14. Rover velocity (directional wheels)

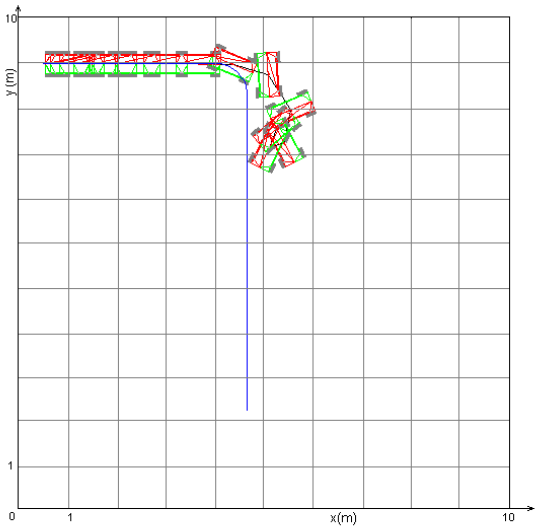

Fig. 15. Right bend (kinematic control)

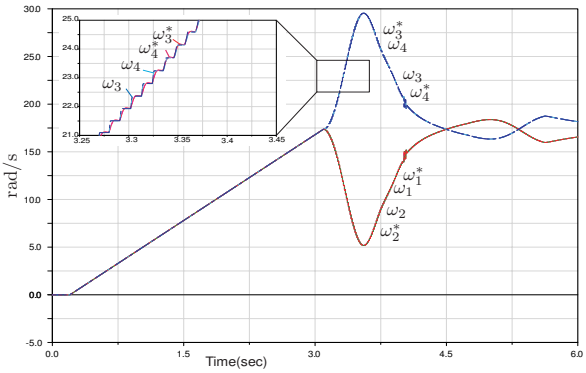

Fig. 16. Wheels angular velocities (kinematic control)

These results show that the trajectory tracking is better for the model-based control under such conditions. The presence of directional wheels allows a better orientation of the tractive efforts, so that the mobility of the system is improved on sliding soils.

We can conclude that the model-based control frame developed in section III has better performances than the pure kinematic control.

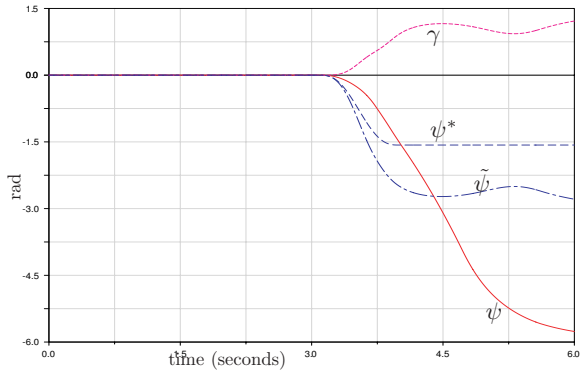

Fig. 17. Rover direction and desired heading (kinematic control)

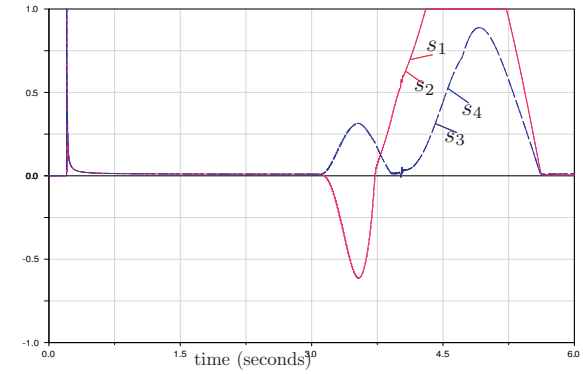

Fig. 18. Slip rates (kinematic control)

VI. Conclusion and perspectives

The controller presented in this paper may be useful to achieve better performances on challenging terrains such as planetary surfaces, but require a larger instrumentation. Obstacle avoidance at high speed is a possible application.

Further works are being made to implement this control strategy in a fast mobile robotic platform, which is under development (Fig. 19). Absolute ground velocity will be measured with a Doppler sensor. Robustness and sensitivity to soil parameters have to be evaluated. Moreover, an off-line nonlinear procedure will be implemented to estimate the soil parameters.

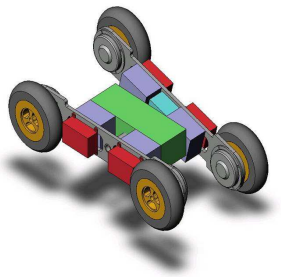

Fig. 19. Skid-steering demonstrator

References

[1] L. Caracciolo, A. De Luca, and S. Iannitti, "Trajectory tracking control of a four-wheel differentially driven mobile robot," in *International Conference on Robotics and Automation*, Detroit, May 1999, pp. 2632–2638, IEEE.

[2] T. Huntsberger, H. Aghazarian, Y. Cheng, E.T. Baumgartner, E. Tunstel, C. Leger, A. Trebi-Ollennu, and P. S. Schenker, "Rover autonomy for long range navigation and science data acquisition on planetary surfaces," in *International Conference on Robotics and Automation*. May 2002, pp. 3161–3168, IEEE.

[3] M. Spenko, K. Iagnemma, and S. Dubowsky, "High speed hazard avoidance for mobile robots in rough terrain," in *SPIE Conference on Unmanned Ground Vehicles*, 2004.

[4] M.G. Bekker, *Introduction to Terrains-Vehicles Systems*, The University of Michigan Press, 1969.

[5] J. Y. Wong, *Terramechanics and Off-Road Vehicles*, Elsevier, 1989.

[6] G. Ishigami, A. Miwa, and K. Yoshida, "Steering trajectory analysis of planetary exploration rovers based on all-wheel dynamics model," in *8th International Symposium on Artifical Intelligence, Robotics and Automation in Space*, Munich, Germany, September 2005.

[7] S.S. Stuchly, A. Thansandote, J. Mladek, and J.S. Townsend, "A doppler radar velocity meter for agricultural tractors," *IEEE Transactions on Vehicular Technology*, vol. 27, no. 1, pp. 24–30, February 1978.

[8] K.R. Buckholtz, "Reference input wheel slip tracking using sliding mode control," in *SAE World Congress Detroit*. Society of Automotive Engineers, march 2002, SAE.

[9] F. Yu, J.-Z. Feng, and J. Li, "A fuzzy logic controller design for vehicle abs with a on-line optimized target wheel slip ratio," *International Journal of Automotive Technology*, vol. 3, no. 4, pp. 165–170, 2002.

[10] J. Kalkkuhl, T. Johansen, and J. Ludemann, "Improved transient performance of nonlinear adaptive backstepping using estimator resetting based on multiple models," *IEEE Trans. Automatic Control*, vol. 47, pp. 136–140, 2002.

[11] K. Yoshida and H. Hamano, "Motion dynamics of a rover with slip-based traction model," in *International Conference on Robotics and Automation*. May 2002, pp. 3155–3160, IEEE.

[12] D. Caltabiano, D. Ciancitto, and G. Muscato, "Experimental results on a traction control algorithm for mobile robots in volcano environment," in *International Conference on Robotics and Automation*, New Orleans, April 2004, pp. 4375–4380, IEEE.

[13] "www.mscsoftware.com/products," MSC Adams.